

Part 4. Recycling Tidal Dwarf Galaxies

The Dynamical Masses of Tidal Dwarf Galaxies

J. E. Hibbard

NRAO, USA

J. E. Barnes

Institute for Astronomy, USA

Abstract. A variety of substructures have been identified within the tidal debris around interacting galaxies. These structures range in scale from Globular Clusters to the so-called “Tidal Dwarf Galaxies”. We review observations of such objects, with particular emphasis on what can be inferred from dynamical mass estimates. We then present the results of a dynamical analysis of structures which develop within the tidal tails of a large- N numerical simulation ($N \sim 1$ million). We find that under the best conditions, “observations” of this system recover the true mass of the bound substructures to within a factor of two. Poor spatial and velocity resolution (coarser than the true half-light radii and velocity dispersions) and more inclined viewing geometries lead the dynamical masses to be over-estimated by factors of ten or more. A combination of poor resolution and edge-on viewing geometries lead to the most dramatic discrepancies, with dynamical masses over-estimated by factors of up to 1000. Furthermore, projection effects can lead to apparent concentrations of material at the ends of tidal tails that is in reality spread over very large distances, with mass scales well beyond that of any truly bound regions. Since many of the well studied tidal dwarf candidates are found within edge-on tails, we conclude that their mass and extent may have been greatly over-estimated.

1. Introduction

Galaxies undergoing violent interactions reveal a wealth of structure, from the brilliant super star clusters shining within their inner regions, to the large-scale tidal tails extending dozens of kiloparsecs. Among these structures are concentrations of gas, light, and/or star forming regions found beaded along or often at the end of filamentary tidal tails. These concentrations range in size from star clusters (Knierman et al. 2003, Tran et al. 2003, de Grijs et al. 2003), to giant H II regions (Hutchings 1996; Weilbacher et al. 2000, 2003), to proto-cluster gas clumps (English et al. 2003), up to the scale of dwarf galaxies (e.g. Mirabel, Dottori & Lutz 1992, Duc et al. 1997, 2000).

Such concentrations have been known for quite some time (e.g. Zwicky 1956, Schweizer 1978), but have only recently received detailed attention. Sev-

eral numerical studies lend support to the hypothesis that self-gravitating condensations can form within tidal debris (Barnes & Hernquist 1992, Elmegreen, Kaufmann & Thomasson 1993), but the supporting observational evidence is primarily circumstantial. These observations show that the condensations contain many young stars (Schweizer 1978, Mirabel et al. 1992, Hunsberger, Charlton, & Zaritsky 1998, Weilbacher et al. 2000, Iglesias-Páramo & Vílchez 2001, Saviane, Hibbard & Rich 2003) and have global properties, such as size, luminosity, H I mass, H I velocity dispersion, and CO content, in common with dwarf Irregular galaxies (Mirabel, Dottori, & Lutz 1992; Hibbard et al. 1994; Smith & Higdon 1994; Duc & Mirabel 1994; Malphrus et al. 1997; Duc et al. 1997, 2000; Braine et al. 2000, 2001). For these reasons, such concentrations are often referred to as “Tidal Dwarf Galaxies” (hereafter TDGs). Recently, some tidal dwarf candidates have even been found to harbor “Super Star Clusters” (Knierman et al. 2004, Saviane et al. 2004).

Since these features form from material previously residing in the disks of the progenitor spirals, the expectation is that they should have a low dark-matter content, or equivalently a low mass-to-light ratio (M/L; Hunter, Hunsberger & Roye 2000). However, the limited observational evidence on TDG candidates suggests quite the opposite, with reported M/L in the range of 4–20 $M_{\odot} L_{\odot}^{-1}$ (e.g. Hibbard et al. 1994, Mendes de Oliveira et al. 2001, Temporin et al. 2003 and these proceedings). The stellar populations within the progenitor disks should have had a considerably lower M/L ($< 2 M_{\odot} L_{\odot}^{-1}$), especially in light of the young stars and star forming regions used to identify most TDG candidates. More remarkably, recent observations measure velocity gradients of 300–400 km s^{-1} across several TDG candidates (Weilbacher et al. 2002, 2003), suggesting M/L ratios of >100 and masses larger than $10^{10} M_{\odot}$. If these kinematics truly reflect gravitational motion, then the concentrations must contain a substantial amount of dark matter¹. Furthermore, for dark matter to be retained by these concentrations it needs to be both dynamically cold and concentrated toward the disk. In other words, one must conclude that there was a substantial dark matter component within the disks of the progenitors (e.g. Pfenniger et al. 1994 and these proceedings). The alternative is that the kinematic measurements are somehow in error, or that they do not accurately reflect the size of the underlying potential.

To address the latter point, we use a large-N numerical simulation for the interacting galaxy NGC 4676 ($N=1,048,576$, Barnes 2003), identify bound regions within the developing tail, and compare “observed” dynamical mass estimates of these condensations to their true mass.

¹Braine et al. (2001 and these proceedings) argue that many TDG candidates are bound by baryons alone. Their calculations evaluate dynamical mass using CO linewidths, while their baryonic mass estimates include a substantial contribution from neutral hydrogen. However, the neutral hydrogen has a much higher velocity dispersion than the CO and therefore would not be confined in the potential traced by the CO. So either the dynamical mass has been greatly under-estimated or the baryonic mass has been greatly over-estimated in these regions.

2. Simulated Observations

The N-body model used in this investigation is that run by Barnes (2003). The progenitor galaxy models consisted of an exponential disk and a bulge embedded in a spherical halo. The number of particles in each component was [262,144:196,608:65,536] for the [halo:disk:bulge], and the total mass of each component was [1.0:0.1875:0.04]. The mass ratio of the two progenitors was set equal to unity, and they were initially set on a prograde parabolic orbit. The encounter geometry was varied to match to the H I data of NGC 4676, “The Mice” (Hibbard & van Gorkom 1996).

The encounter develops in the standard way, with each system throwing off a large tidal tail (see Sparke & Gallagher 2000, Fig. 5.37 for snapshots of a lower-N rendition of this encounter). Within each tail, small condensations form as the tails are ejected, exactly analogous to the manner documented by Barnes & Hernquist (1992; hereafter BH92).

For this investigation we looked at a late stage of the encounter, when the contrast between bound regions within the tail and the surrounding tidal material is large. When using scaling parameters suitable for matching the H I observations of The Mice, this time corresponds to 800 Myr after first pericenter. At this stage the progenitor disks have merged and the tails stretch to a radius of 200 kpc. With these scaling parameters each progenitor has a total mass of $4.6 \times 10^{11} M_{\odot}$, and each disk particle corresponds to a mass of $3.5 \times 10^5 M_{\odot}$.

Following BH92, we identify bound regions within the tails using a friends-of-friends algorithm and identifying all particles near local potential minima which have a ratio of kinetic to potential energy less than -0.5 so that they are approximately virialized. This procedure identifies 64 bound entities within the tails, with masses ranging from $3 \times 10^6 M_{\odot}$ to $4 \times 10^8 M_{\odot}$ (unshaded histogram in Figure 1a). In order to have a reasonable chance to accurately measure a half-light radius and velocity dispersion and thus to derive a virial mass, we consider only those regions which (1) contain more than 50 particles; (2) have a well defined density maxima; and (3) are roughly spherical in shape. This results in a sample of 18 well-localized TDG candidates. The mass, half-light radius, and velocity dispersion of each of these candidates are indicated by the shaded histograms in Fig. 1.

The simulation was “observed” by specifying a viewing geometry, a spatial cell size, and a line-of-sight velocity binning width. Moments were taken of this observational “cube”, with the zeroth moment map corresponding to all particles in a spatial cell summed over velocity (i.e. total intensity map), and the second moment map corresponding to the velocity dispersion of all particles in a cell (i.e. intensity weighted velocity dispersion). Examples of a zeroth moment map of the simulation for two different viewing geometries is given in Figure 3, with the top panel showing a view looking down upon the orbital plane, and the bottom panel showing a more edge-on view.

The half-light radii of each clump was measured from the zeroth moment map, and the velocity dispersion was measured from the second moment map. The virial mass was then estimated via the formula $M_{vir} = 3\sigma^2 ar_{1/2}G^{-1}$, where G is the gravitational constant, σ is the (1-dimensional) velocity dispersion, the factor 3 assumes that the velocity dispersion is isotropic, $r_{1/2}$ is the projected

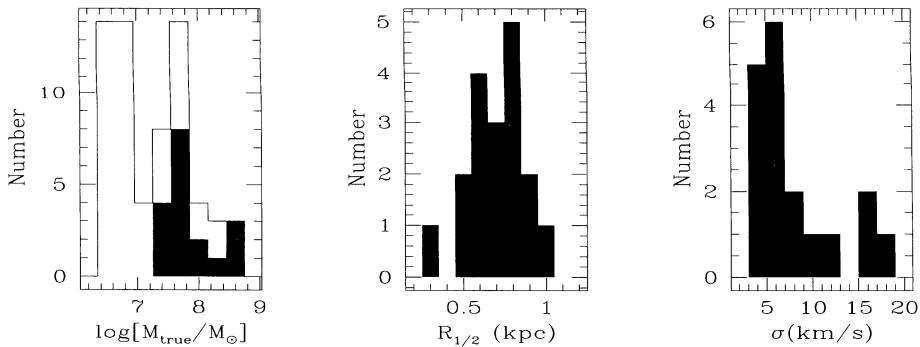


Figure 1. Histograms of physical characteristics of bound structures which formed within the tails of the numerical simulation of “The Mice”. Left panel: range of masses. Unfilled histogram represents the values for 64 identified structures, while the shaded histogram represents a sub-sample of 18 well-localized sources. The following two panels plot the half light radii and velocity dispersions of the well-localized sources.

half-light radius, and a is a geometric factor, which is 2.7 for an isothermal sphere.

We tested how well this virial mass estimate recovers the true mass of each candidate as the spatial cell size, velocity binning width, and viewing perspective was varied. Figure 2 presents the results of these studies. In each panel we plot the ratio of the virial mass to the true mass of each condensation. In the left panel the true half-light radius of each clump is plotted in units of the spatial cell spacing. No velocity binning is used, and the tails are viewed from a face-on viewing geometry (top panel of Fig. 3). In the middle panel the true velocity dispersion is plotted in units of the velocity binning width. The finest spatial binning is used (corresponding to a cellsize of $\Delta x_0 = 430$ pc), and the tails are again viewed from a face-on viewing geometry. In the final panel the rotation angle is measured with respect to the orbital plane, with a rotation angle of 0° corresponding to the top view of Fig. 3. No velocity binning was used. Triangles correspond to measurements made with $\Delta x/\Delta x_0 = 1$, while squares represent coarser spatial binning. The columns of squares at rotation angles of 20° and 50° have $\Delta x/\Delta x_0 = 2$, while the column at a rotation angle of 100° has $\Delta x/\Delta x_0 = 4$. This last column represents the case illustrated in the bottom panel of Fig. 3.

These plots show that when the simulation is “observed” with good spatial and velocity sampling (spatial resolution smaller than or equal to the half-light radius; velocity resolution smaller than or equal to the velocity dispersion) and

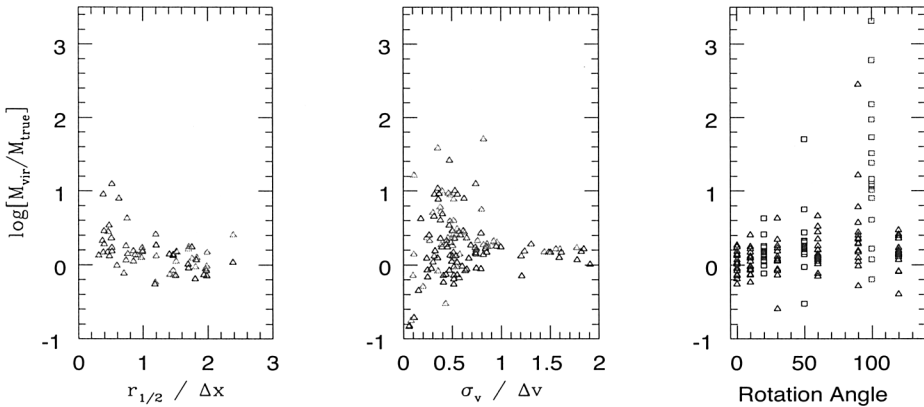


Figure 2. Effect of spatial resolution, velocity resolution, and viewing angle on the ratio of the derived virial mass to the true mass of each of the bound regions within the tails. The leftmost panel presents the results of varying the spatial resolution; the middle panel presents the results of varying the velocity binning, and the rightmost panel presents the results of varying the viewing geometry.

from face-on viewing geometries, the virial mass estimate reproduces the true mass to within a factor of two. However, the virial mass estimates become very unreliable when the simulation is observed with poor spatial or velocity resolution, or when viewed from inclined viewing geometries. Under these conditions, the virial mass consistently over-estimates the true mass, often by factors of 10 and occasionally by factors of several hundred.

The greatest scatter is found for nearly edge-on viewing perspectives with poor spatial resolution (column at rotation angle=100° in Fig. 2c). This case is shown in more detail in Fig. 3, where we have identified the location of each of the 18 well-localized bound regions within the tails. The numbers give the ratio of the virial to true mass for each bound region. The spatial cell-size in the bottom case corresponds to 1.6 kpc. This shows that line-of-sight effects lead to very unreliable mass determinations when the tail is inclined, with over-estimates by factors of 10–1000. This is simply because at these viewing geometries non-bound material is projected against the bound regions, increasing both the measured half-light radius and velocity dispersion.

The above analysis assumes that the locations of the bound regions are actually known. In practice, observers usually identify concentrations of light and gas and measure their properties. For instance, it would be typical to identify the region outlined by the dotted line in the bottom panel of Fig. 3.

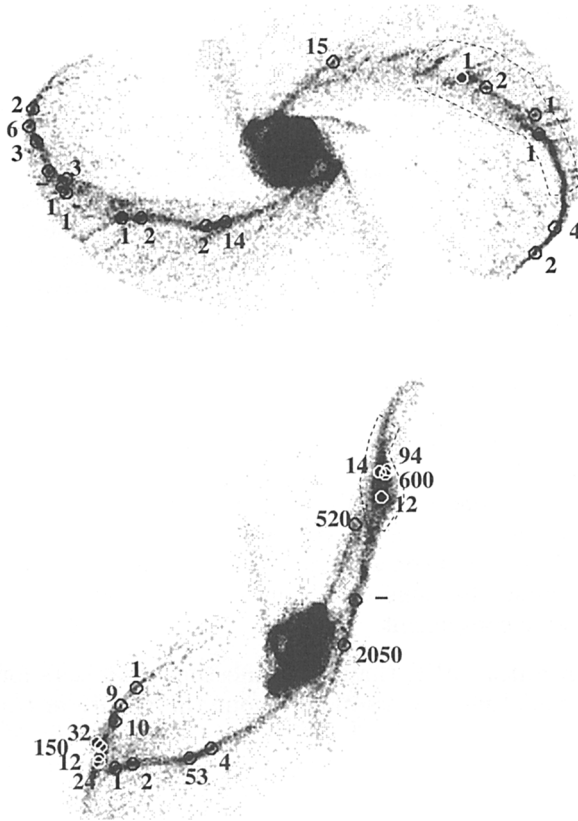


Figure 3. Face-on (top) and more edge-on (bottom) view of simulation. Each of the bound knots within the tails are circles, with the adjacent numbers indicating the ratio of the derived virial to true mass. The dotted line in the bottom panel outlines a region which might typically be identified as a tidal dwarf candidate.

Material which contributes to this concentration is identified by a dotted line in the top panel, showing that it comes from a very large region spread along the line of sight. The actual mass of the particles contributing to this concentration amounts to $5 \times 10^9 M_{\odot}$, much larger than any of the regions which are actually bound.

3. Conclusions

In light of this study, we conclude that, even under the best conditions, one should not expect dynamical mass estimates of tidal dwarf candidates to be good to better than a factor of two. Poor spatial and velocity resolution (coarser than the true half-light radii and velocity dispersions) and more inclined viewing geometries lead the dynamical mass to be over-estimated by factors of ten or

more. A combination of poor resolution and edge-on viewing geometries lead to the most dramatic discrepancies, with dynamical masses over-estimated by factors of up to 1000. Furthermore, projection effects can lead to apparent concentrations of material at the ends of tidal tails that is in reality spread over very large distances, with mass scales well beyond that of any truly bound regions.

We therefore suspect that most tidal dwarf galaxies are much smaller than generally advertised, with masses more like $10^7 - 10^8 M_{\odot}$ than the more commonly claimed $10^9 - 10^{10} M_{\odot}$. It is notable that many of the best studied tidal dwarf candidates are viewed from unfavorable perspectives (e.g., Arp 105 Duc et al. 1994, 1997; NGC 4038/9 Mirabel et al. 1992, Hibbard et al. 2001; Arp 245 Duc et al. 2000, Brinks these proceedings; NGC 4676 Amram, Bournaud and Duc these proceedings). Many of these may consist of unbound material projected to appear like mass concentrations.

Still, self-gravitating regions *are* expected to form within tidal tails, and some of these may be long-lived entities. If dark matter halos are roughly spherical, then such concentrations are expected to have a low dark matter content. To test this conclusion, one need only to measure dynamical masses for concentrations in less-inclined tidal tails. We predict that these mass estimates will be much smaller than has been inferred so far. If large dynamical masses are still inferred for these, then one must consider the possibility of a substantial disk-like dark-matter component.

Acknowledgments. JEH thanks the meeting organizers for the invitation and for many stimulating conversations about the nature of tidal dwarfs near the pier in Sydney.

References

- Barnes, J. E. 2003, MNRAS, submitted²
- Barnes, J. E., & Hernquist, L. 1992, *Nature*, 360, 715
- Braine, J., Duc, P.-A., Lisenfeld, U., Leon, S., Vallejo, O., Charmandaris, V. & Brinks, E. 2001, *A&A*, 378, 51
- Braine, J., Lisenfeld, U., Duc, P.-A., & Leon, S., 2000, *Nature*, 403, 867
- de Grijs, R., Lee, J.T., Clemencia Mora Herrera, M., Fritze-v. Alvensleben, U., Anders, P. 2003, *New Ast.*, 8, 155
- Duc, P. -A., Mirabel, I. F. 1994, *A&A*, 289, 83
- Duc, P. -A., Brinks, E., Wink, J. E., & Mirabel, I. F. 1997, *A&A*, 326, 537
- Duc, P. -A., Brinks, E., Springel, V., Pichardo, B., Weilbacher, P., & Mirabel, I.F., 2000, *AJ*, 120, 1238
- Elmegreen, B., Kaufmann, M., & Thomasson, M. 1993, *ApJ*, 412, 90
- English, J., Norris, R. P., Freeman, K. C., & Booth, R. S. 2003, *AJ*, 125, 1134
- Hibbard, J. E., & van Gorkom, J. H. 1996, *AJ*, 111, 655

²see also <http://www.ifa.hawaii.edu/~barnes/pressrel/mice/>

- Hibbard, J. E., Guhathakurta, P., van Gorkom, J. H., & Schweizer, F. 1994, AJ, 107, 67
- Hibbard, J. E., van der Hulst, J. M., Barnes, J. E., & Rich, R.M. 2001, AJ, 122, 2969
- Hunsberger, S., Charlton, J., & Zaritsky, D. 1998, ApJ, 505, 536
- Hunter, D. A., Hunsberger, S., & Roye, E.W. 2000, ApJ, 542, 137
- Hutchings, J. B. 1996, AJ, 111, 712
- Iglesias-Páramo, J., & Vilchez, J. M. 2001, ApJ, 550, 204
- Knierman, K. A., Gallagher, S. C., Charlton, J. C., Hunsberger, S. D., Whitmore, B., Kundu, A., Hibbard, J. E., & Zaritsky, D. 2004, AJ, in press
- Malphrus, B. K., Simpson, C. E., Gottesman, S. T., & Hawarden, T. G. 1997, AJ, 114, 1427
- Mendes de Oliveira, C., Plana, H., Amram, P., Balkowski, C., & Bolte, M., 2001, AJ, 121, 2524
- Mirabel, I. F., Dottori, H., & Lutz, D. 1992, A&A, 256, L19
- Pfenniger, D., Combes, F., & Martinet, L. 1994, A&A, 285, 79
- Saviane, I., Hibbard, J.E. & Rich 2004, AJ, in press
- Schweizer, F. 1978, The Structure and Properties of Nearby Galaxies, IAU Symp. No. 77, edited by E. M. Berkhuijsen and R. Wielebinski (Reidel, Dordrecht), 279
- Smith, B. J., & Higdon, J. L. 1994, AJ, 108, 837
- Sparke, L.S. & Gallagher, J.S. III 2000, *Galaxies in the Universe: an Introduction*, (Cambridge: Cambridge Univ. Press)
- Temporin, S., Weinberger, R., Galaz, G., & Kerber, F. 2003, ApJ, 587, 660
- Tran, H. D. et al. 2003, 585, 750
- Weilbacher, P. M., Duc, P.-A., Fritze-v.Alvensleben, U., Martin, P., & Fricke, K. J. 2000, A&A, 358, 819
- Weilbacher, P. M., Duc, P.-A., & Fritze-v.Alvensleben, U. 2003, A&A, 397, 545
- Weilbacher, P. M., Fritze-v.Alvensleben, U., Duc, P.-A., & Fricke, K. J. 2002, ApJ, 579, L79
- Zwicky, F. 1956, *Ergebnisse der Exakten Naturwissenschaften*, 29, 344